

Fluid Flow over a Sharp and Blunt V-shaped Region

I. A. Ismail¹ and Gihan. E. H. Ali²

Tok tekutiny ostro lomeným potrubím v tvare V

In this paper we study a viscous fluid flow over a V-shaped body for a range of Reynold's number from $Re = 5$ up to $Re = 500$. We solved the unsteady Naveir-stokes equations in the stream function - vorticity formulation. The irregular physical domain is transformed into a rectangular shape using the elliptic grid generation. We applied the Finite difference discretization technique for governing the partial differential equations, in this technique, the computational domain is covered by a pattern, network or mesh points called grid points. The governing equations are then reformulated at each interior point by replacing all partial derivatives with appropriate Finite differences, thus converted to a set of discrete algebraic equations.

Key words: successive-over relaxation iteration method, Naveir-Stokes equations, Stream function-Vorticity formulation, Grid Generation

Introduction

In most frequently encountered situations, fluid flows can be classified into different categories according to their density and viscosity. For the compressible flows the variation of density must be taken into account which implies that $M > 0.1$, where M is the Mach number (the local speed of sound); conversely, for the incompressible flows, the flow speeds are assumed to be much smaller than the speed of sound, i.e $M \ll 1$. On the other hand, the consideration of the influence of viscosity suggests three major categories: inviscid flow with the zero dynamic viscosity; the boundary layer flow, where the viscosity is important in the vicinity of the surface; and the separated flow, where the viscosity is important in the whole concerned region. There are other points of view to categorize the fluid flow, mathematically and numerically. First, mathematically, the criteria could be the type of the governing PDE or the method of the solution of the governing equations. Second, regarding the geometric configuration, there are three categories: flows outside bodies; confined flows and partially confined flows. From the numerical analysis point of view, the principal tasks of the CFD are the following:

- the first one is concerned with the governing equations and the associated initial and boundary conditions which are replaced by a system of algebraic equations through the discretization techniques,
- the second one are the algebraic equations produced by the discretizations, which are solved using an efficient computational method.

Formulation of The Problem - Governing Equations

The Streamfunction-Vorticity form of the unsteady NS equations are given in [1] by:

$$\psi_{xx} + \psi_{yy} = -\zeta \quad (1)$$

$$\zeta_t + \psi_y \zeta_x - \psi_x \zeta_y = \frac{1}{Re} (\zeta_{xx} + \zeta_{yy}) \quad (2)$$

where ψ is the stream function, ζ the vorticity, and Re is the non-dimensional Reynolds number. The important feature of the stream function-vorticity formulation is that the pressure P is not found explicitly in these equations.

The equations:

$$u = \psi_y \quad v = -\psi_x \quad (3)$$

are the velocity components at any point of a two-dimensional flow. The graphs of the physical domain are shown in the figure (1) and (2).

Grid system for the contraction geometry (Graph of the blunt V-shape) 41 x 41 grid points.

¹ I. A. Ismail, Faculty of Computing and Informatics, Zagazig University, Egypt

² Gihan. E. H. Ali, Faculty of Petroleum and Mining engineering, Suez Canal University, Suez, Egypt, j3aziza@yahoo.com
(Recenzovaná a revidovaná verzia dodaná 3. 8. 2005)

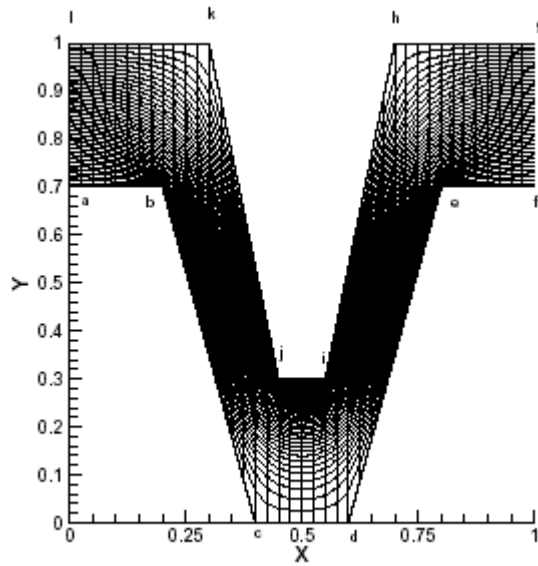


Fig. 1. Grid system on the blunt V-shaped domains 2

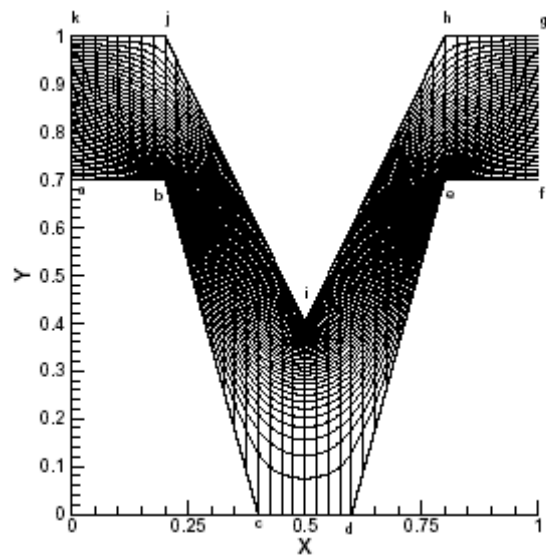


Fig. 2. Grid system on the sharp V-shaped domain

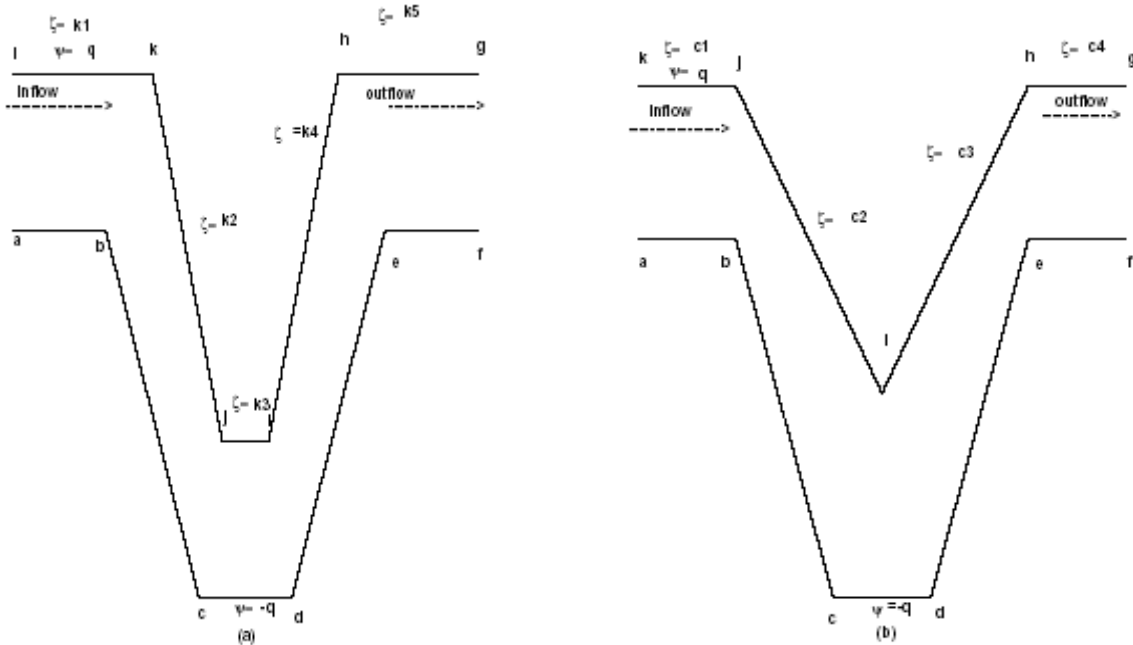


Fig. 3. The flow direction through the physical domain

Numerical grid generation - mathematical development

In the present work we study the incompressible fluid flow in the V shape geometry, which is a non rectangular domain, using the Numerical Grid Generation to overcome the difficulty of the nonequal step sizes of the grid points [9] and [10].

To overcome this difficulty some general mappings were employed to transform the non-rectangular physical domain into the rectangular computational domain. These transformations lead to a uniformly grid spacing in the computational plane while points in the physical space may be unequally spaced by specifying the generalized coordinate system, that will map the non-rectangular grid system in the physical space to a rectangular uniform grid spacing in the computational space. The central issue at this point is to identify the location of the grid points in the physical domain. That is, what are the x and y coordinates of a grid point in the physical space that correspond to a grid point (i; j) specified in the computational domain?. Here, a system of elliptic equations in the form of Laplace equations is introduced, which is solved for grid points in the physical domain. The general transformation from the physical plane x; y to the transformed plane ξ, η is:

$$\xi = \xi(x, y) \quad , \eta = \eta(x, y) \tag{4}$$

$$\begin{aligned}\xi_x &= (1/J)y_\eta, \xi_y = (-1/J)x_\eta \\ \eta_x &= (-1/J)y_\xi, \eta_y = (1/J)x_\xi \\ J &= x_\xi y_\eta - x_\eta y_\xi.\end{aligned}\tag{5}$$

Now, for any function f , the first derivative in the computational domain is given by:

$$f_x = (1/J)[y_\eta f_\xi - y_\xi f_\eta]\tag{6}$$

and the Laplacian is defined as :

$$\nabla^2 f = (1/J^2)(\alpha f_{\xi\xi} - 2\beta f_{\xi\eta} + \gamma f_{\eta\eta} + df_\eta + ef_\xi)\tag{7}$$

where $\alpha, \beta, \gamma, d, e$ are as given in [9].

For any function $f(x,y)$ the transformation of the time derivative from the physical domain to the computational domain takes the form:

$$\begin{aligned}\left(\frac{\partial f}{\partial t}\right)_{x,y} &= \left(\frac{\partial f}{\partial t}\right)_{\xi,\eta} + (1/J)[y_\xi f_\eta - y_\eta f_\xi]x_t \\ &+ (1/J)[x_\eta f_\xi - x_\xi f_\eta]y_t.\end{aligned}\tag{8}$$

The system of elliptic equations:

$$\begin{aligned}\alpha x_{\xi\xi} - 2\beta x_{\xi\eta} + \gamma x_{\eta\eta} &= 0 \\ \alpha y_{\xi\xi} - 2\beta y_{\xi\eta} + \gamma y_{\eta\eta} &= 0\end{aligned}\tag{9}$$

is solved in the computational domain (ξ,η) in order to provide the grid point locations in the physical space (x,y) .

$$\begin{aligned}\psi_x &= (1/J)[y_\eta \psi_\xi - y_\xi \psi_\eta] \\ \psi_y &= (1/J)[x_\xi \psi_\eta - x_\eta \psi_\xi] \\ \zeta_x &= (1/J)[y_\eta \zeta_\xi - y_\xi \zeta_\eta] \\ \zeta_y &= (1/J)[x_\xi \zeta_\eta - x_\eta \zeta_\xi] \\ \left(\frac{\partial \zeta}{\partial t}\right)_{x,y} &= \left(\frac{\partial \zeta}{\partial t}\right)_{\xi,\eta} + (1/J)[y_\xi \zeta_\eta - y_\eta \zeta_\xi]x_t \\ &+ (1/J)[x_\eta \zeta_\xi - x_\xi \zeta_\eta]y_t.\end{aligned}\tag{10}$$

The spatial derivatives are obtained in the non conservative form, i.e: $[\zeta_t]_{xy} = [\zeta_t]_{\xi\eta} - (\zeta_x x_t + \zeta_y y_t)$, putting $x_t = y_t = 0$ [19], so that $[\zeta_t]_{\xi\eta} = [\zeta_t]_{xy}$. The equations in the physical domain are now transformed into the ξ,η plane and thus all the computations will be performed in the computational domain. Thus, the governing equations in the computational domain will have the form:

$$\zeta_t + \frac{1}{J}(\psi_\eta \zeta_\xi - \psi_\xi \zeta_\eta) = \frac{1}{Re}(1/J^2)(\alpha \zeta_{\xi\xi} - 2\beta \zeta_{\xi\eta} + \gamma \zeta_{\eta\eta} + d\zeta_\eta + e\zeta_\xi)\tag{12}$$

$$(1/J^2)(\alpha \psi_{\xi\xi} - 2\beta \psi_{\xi\eta} + \gamma \psi_{\eta\eta} + d\psi_\eta + e\psi_\xi) = -\zeta\tag{13}$$

$$u = \psi_y = (1/J)[x_\xi \psi_\eta - x_\eta \psi_\xi] \quad (14)$$

$$-v = \psi_x = (1/J)[y_\eta \psi_\xi - y_\xi \psi_\eta]$$

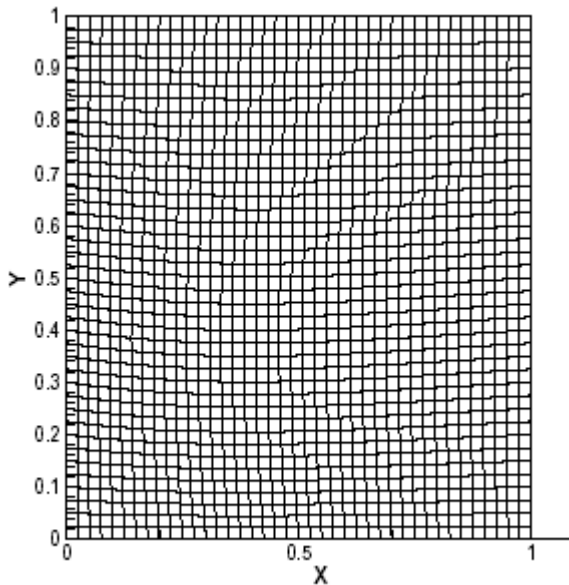


Fig. 4. Grid system on the computational domains

To solve numerically equations (12), (13) and (14) with the boundary conditions as shown in Fig. 3., we use the second order central finite difference formulae, given by:

$$f_{\xi\xi}|_{i,j} = \frac{f(i+1,j) - 2f(i,j) + f(i-1,j)}{\Delta\xi^2} \quad (15)$$

$$f_{\eta\eta}|_{i,j} = \frac{f(i,j+1) - 2f(i,j) + f(i,j-1)}{\Delta\eta^2}$$

and the first derivatives

$$f_\xi|_{i,j} = \frac{f(i+1,j) - f(i-1,j)}{2\Delta\xi} \quad (16)$$

$$f_\eta|_{i,j} = \frac{f(i,j+1) - f(i,j-1)}{2\Delta\eta}$$

On the boundaries we use the second-order finite difference approximation for $\frac{\partial f}{\partial \xi}$ and $\frac{\partial f}{\partial \eta}$, which is given by:

$$f_\xi|_{i,j} = \frac{-f(i+2,j) + 4f(i+1,j) - 3f(i,j)}{2\Delta\xi} \quad (17)$$

$$f_\eta|_{i,j} = \frac{-f(i,j+2) + 4f(i,j+1) - 3f(i,j)}{2\Delta\eta}$$

$$f_{\xi\eta}|_{i,j} = \frac{f(i+1,j+1) - f(i-1,j+1) - f(i+1,j-1) + f(i-1,j-1)}{4\Delta\xi\Delta\eta} \quad (18)$$

Similarly, we can find the first and second derivatives for V and P. The time derivative terms are approximated using the forward difference approximation, which takes the form

$$f_t|_{i,j} = \frac{f^{n+1}(i,j) - f^n(i,j)}{\Delta t} \quad (19)$$

see [14] and [4]. The difference equations can be

obtained by applying equations (15), (18) to equations (11), (14).

$$\begin{aligned} & \frac{\zeta^{k+1}(i, j) - \zeta^k(i, j)}{\Delta t} + \frac{1}{4J_{i,j}\Delta\eta\Delta\xi}[(\psi^k(i, j+1) - \psi^k(i, j-1))(\zeta^k(i+1, j) - \zeta^k(i-1, j))] \\ & - (\psi^k(i+1, j) - \psi^k(i-1, j))(\zeta^k(i, j+1) - \zeta^k(i, j-1)) = \frac{\alpha_{i,j}}{ReJ_{i,j}^2(\Delta\xi)^2}[\zeta^k(i+1, j) \\ & - 2\zeta^k(i, j) + \zeta^k(i-1, j)] - \frac{\beta_{i,j}}{2\Delta\xi\Delta\eta ReJ_{i,j}^2}[\zeta^k(i+1, j+1) + \zeta^k(i-1, j-1) \\ & - \zeta^k(i+1, j-1) - \zeta^k(i-1, j-1)] + \frac{\gamma_{i,j}}{ReJ_{i,j}^2\Delta\eta^2}[\zeta^k(i, j+1) - 2\zeta^k(i, j) + \zeta^k(i, j-1)] \\ & + \frac{d_{i,j}}{2J_{i,j}^2 Re\Delta\eta}[\zeta^k(i, j+1) - \zeta^k(i, j-1)] + \frac{e_{i,j}}{2J_{i,j}^2 Re\Delta\xi}[\zeta^k(i+1, j) - \zeta^k(i-1, j)] \end{aligned} \quad (20)$$

$$\begin{aligned} & \frac{\alpha_{i,j}}{ReJ_{i,j}^2(\Delta\xi)^2}[\psi(i+1, j) - 2\psi(i, j) + \psi(i-1, j)] - \frac{\beta_{i,j}}{2\Delta\xi\Delta\eta ReJ_{i,j}^2}[\psi(i+1, j+1) + \psi(i-1, j-1) \\ & - \psi(i+1, j-1) - \psi(i-1, j-1)] + \frac{\gamma_{i,j}}{ReJ_{i,j}^2\Delta\eta^2}[\psi(i, j+1) - 2\psi(i, j) + \psi(i, j-1)] \\ & + \frac{d_{i,j}}{2J_{i,j}^2 Re\Delta\eta}[\psi(i, j+1) - \psi(i, j-1)] + \frac{e_{i,j}}{2J_{i,j}^2 Re\Delta\xi}[\psi(i+1, j) - \psi(i-1, j)] = -\zeta(i, j) \end{aligned} \quad (21)$$

Similarly we can get the difference equations for u and v.

Discussion of the results

Two regions of the fluid flow are under consideration. These two regions differ in that their upper border is either of blunt or sharp 'V' shape, see fig. 1. and 2.. So that each of the flow attributes corresponding to any specified Reynold's number is displayed for these two cases, respectively for Re = 5. Figure 5. gives the streamlines for the flow. In Fig 5a, we observe that at the entrance to the region there is some small vortex formed at the left corner, while at the exit where the flow starts to slow down, the area of the vortex increases where continues to slow down due to the gravity and the deceleration due to the flow along the flat edge of the upper border. In Fig 5b, the streamlines are more or less symmetrical, except at the exit, where the slow down is at maximum. The same comments are applied to the rest of cases up to Re = 500, see figures 6- 12. Nevertheless, the vortices at different points in the flow region are given, which have a maximum gradient at points where the flow starts to slow down, as expected at the exit of the flow region. The vorticities are computed for Re = 5 up to Re = 500. It is worthwhile noting that after Re = 300 the viscosity of the fluid in general becomes less and the gradient of the vorticity on the exit side becomes weaker as Re increases. It looks from the above results that our model is in a very reasonable accordance with the physical state of the flow for different Reynold's numbers.

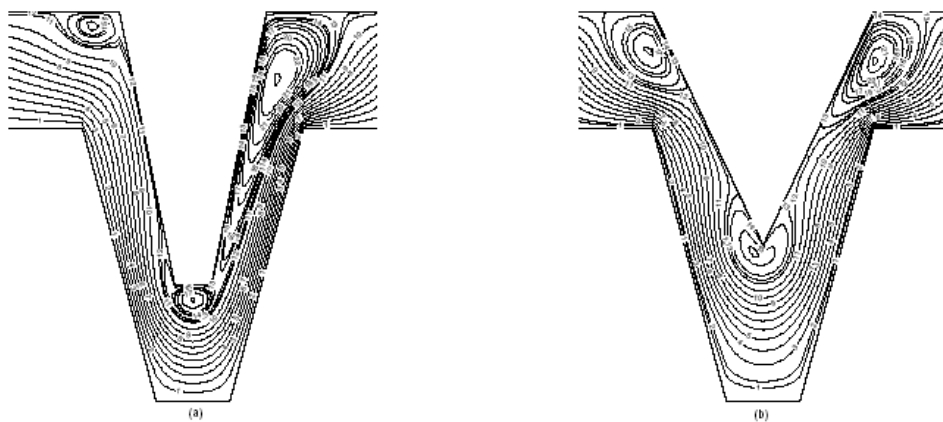


Fig. 5. The graph of ψ at Re = 5

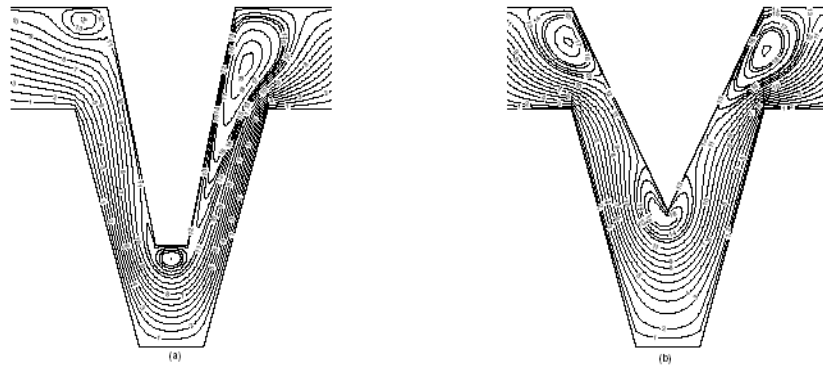


Fig. 6. The graph of ψ at $Re = 10$

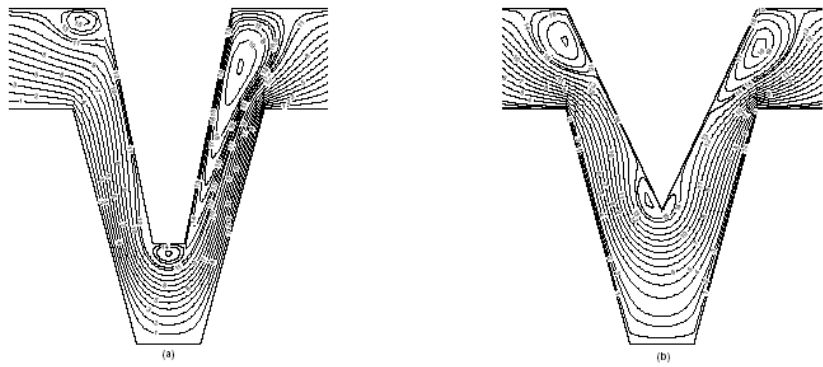


Fig. 7. The graph of ψ at $Re = 50$

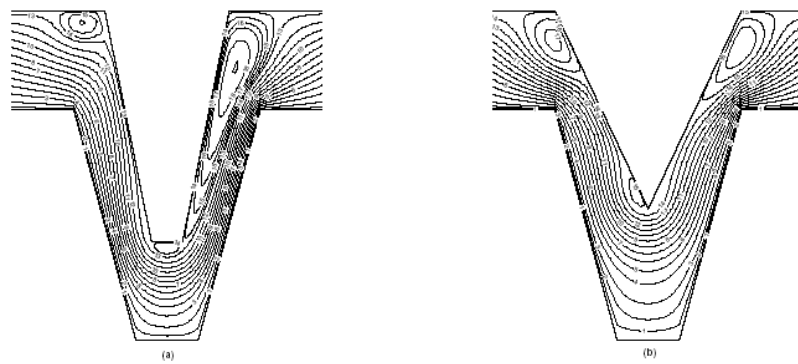


Fig. 8. The graph of ψ at $Re = 100$

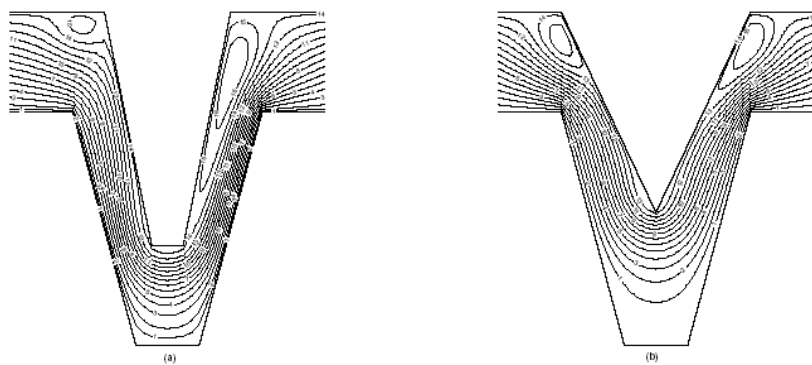


Fig. 9. The graph of ψ at $Re = 200$

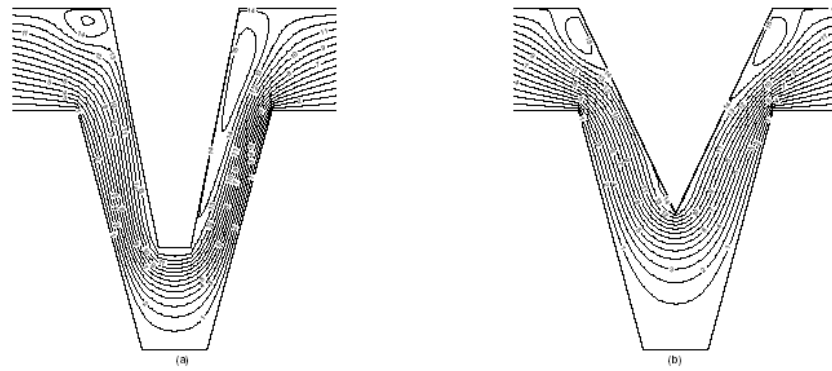


Fig. 10. The graph of ψ at $Re = 300$

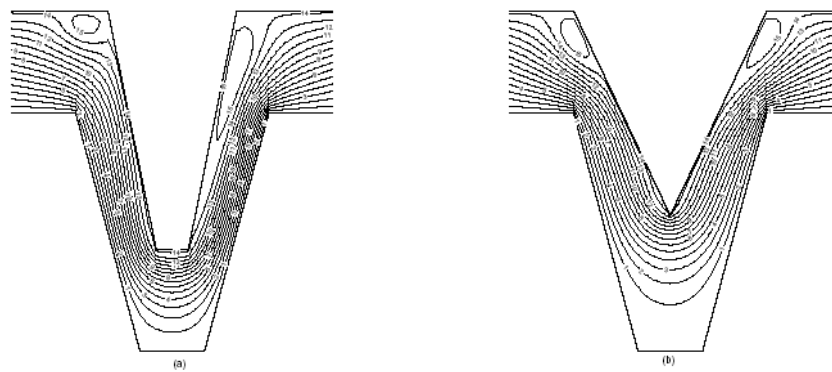


Fig. 11. The graph ψ $Re = 400$

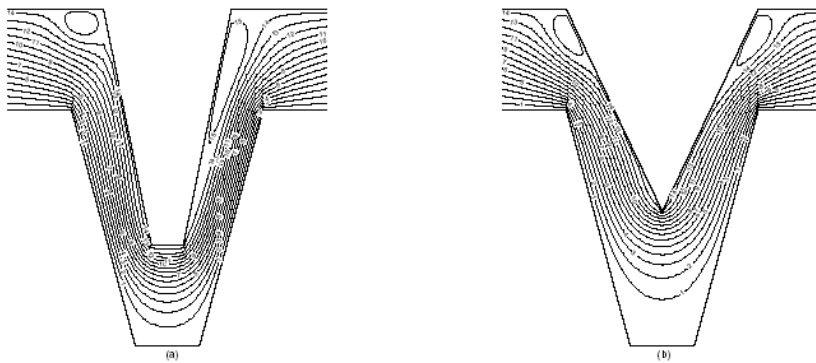


Fig. 12. The graph of ψ at $Re = 500$

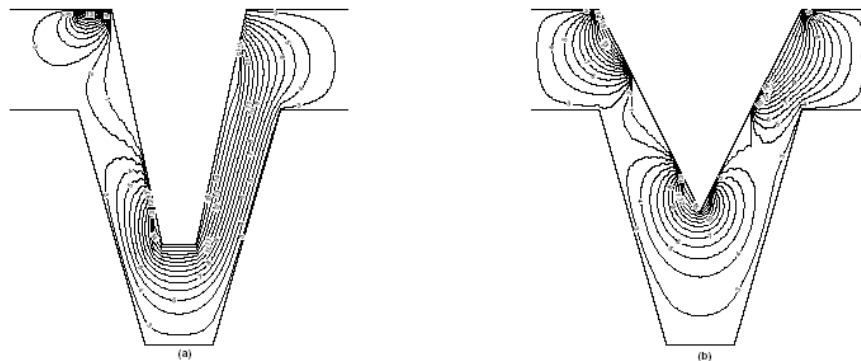


Fig. 13. The graph of ζ at $Re = 5$

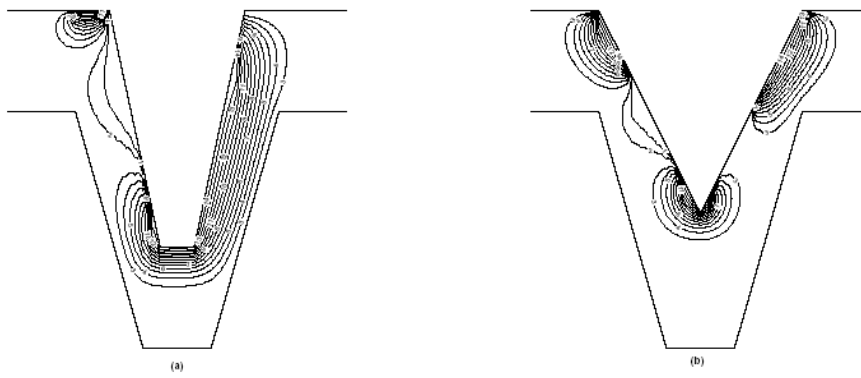


Fig. 14. The graph of ζ at $Re = 10$

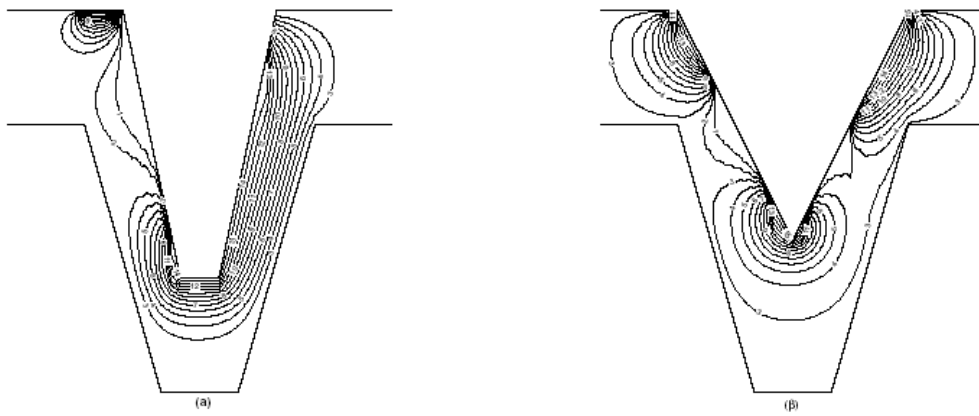


Fig. 15. The graph of ζ at $Re = 50$

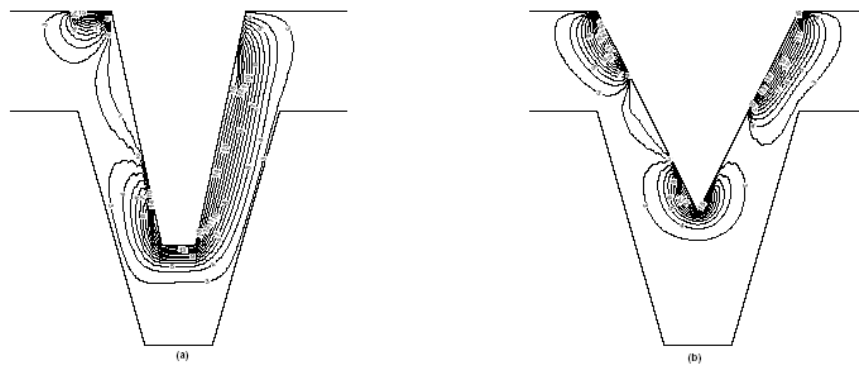


Fig. 16. The graph of ζ at $Re = 100$

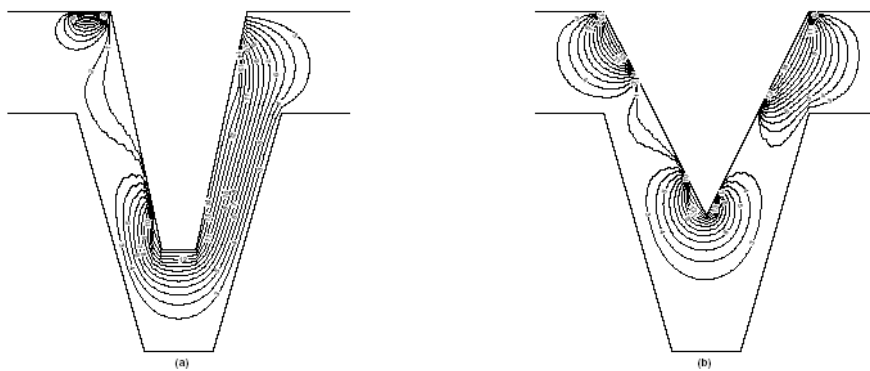


Fig. 17. The graph of ζ at $Re = 200$

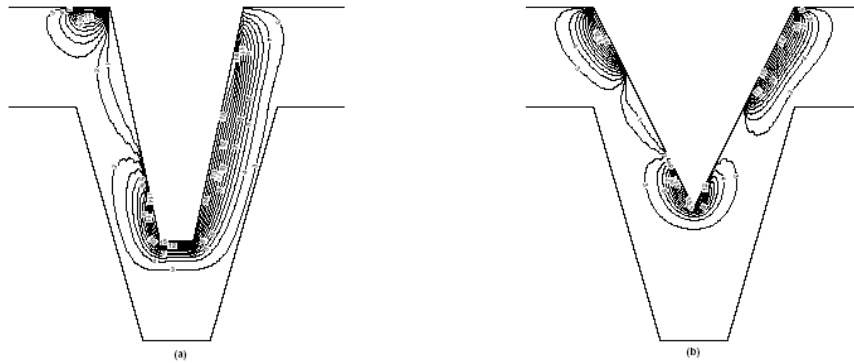


Fig. 18. The graph of ζ at $Re = 300$

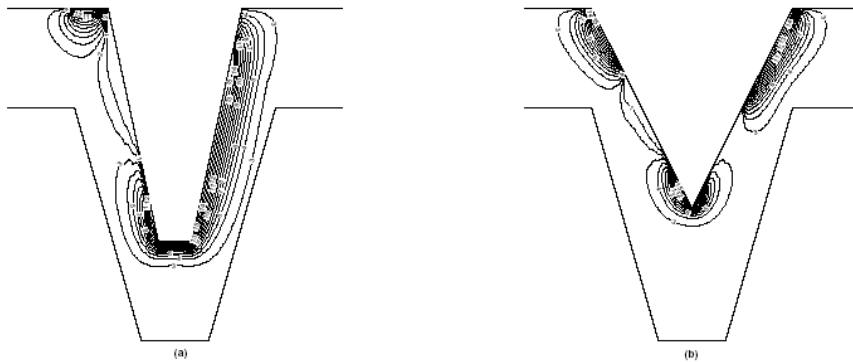


Fig. 19. The graph of ζ at $Re = 400$

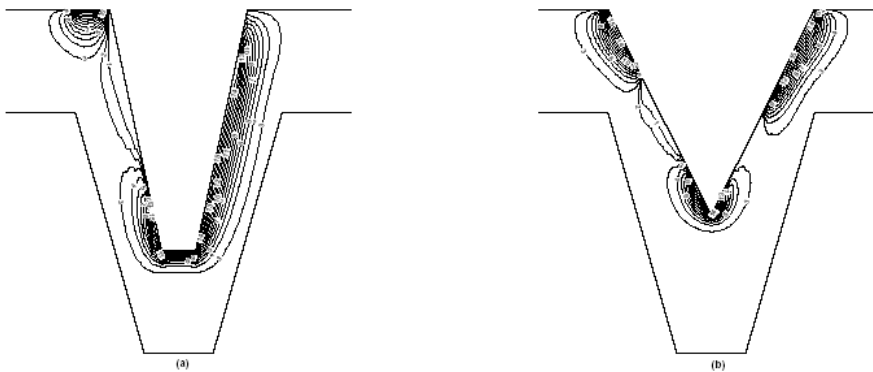


Fig. 20. The graph of ζ at $Re = 500$

References

- [1] Ming Li and Tao Tang: J. Scientific computing , 16 (2001), p. 29-45.
- [2] Amsden A. A and Hirt C. W.: Journal of comp. phys., 11 (1973), p. 348-359.
- [3] Barfield W. D.: Comp.Phys., 5 (1970), p. 23-33.
- [4] Burden R., Faires J., A. Reynolds: Numerical Analysis, Third Edition, Prindle, Weber and Schmidt, Boston, (1985).
- [5] Chu W. H: J. of Comp. Phys., 8 (1971), p. 392-408.
- [6] Eisman P. R.: Ann. Rev. Fluid Mech., 17 (1985), p. 487-521.
- [7] Ghia K. N, Hankey W. L, Jr. and Hodge J. K.: AIAA. J., 643(1977), p. 156-167.
- [8] Haberman R.: Elementary Applied Partial Differential Equations, Prentice-Hall, Englewood Cliff, N.J., (1987).
- [9] Hoffmann K. A: Computational Fluid Dynamics for Engineers, Austin, Texas, (1989).
- [10] Middlecoff J. F and Thomas P. D.: AIAA. J., 18(1980), p. 652-656.
- [11] Plybon B. F: An Introduction to Applied Numerical Analysis , PWS-KENT, Boston, (1992).
- [12] Roach P.: J, computational Fluid Dynamics, Albuquerque, New Mexico, (1982).

- [13] Shanks P. S and Thompson J. F: Proceedings of the 2nd International Conference on Numerical Ship Hydrodynamics, *Berkely*, (1977), p.202-217.
- [14] Smith G. D, Numerical Solution of Partial Differential Equations, *Oxford University Press, Oxford*, (1985).
- [15] Thompson J. F, Ed.: Numerical Grid Generation , *North Holland*(1988).
- [16] Thompson J. F,Ed., Mastin C. W, and Warsi Z. U. A: Numerical Grid Generation, *Elsevier Science Publishing, New York*, (1985).
- [17] Thompson J. F, Ed., Mastin C.W, and Thames F. C.: *J.Comp.Phys.*, 24 (1977), p. 274-303.
- [18] Thompson J. F, Ed., Mastin C.W, and Thames F. C.: *J.comp. phys.*, 15 (1974), p. 299-319.
- [19] Thompson J.F,Ed., Mastin C.W, and Walker R. L.: *J. Comp. Phys.*, 24 (1977), p. 245-273.
- [20] Vinokur M.: *J.Comp.Phys.*, 50 (1983), p. 215-234.
- [21] Warsi Z. U. A and Thompson J. F: Machine solutions of partial differential equations in the numerically generated coordinate systems, *MSSU-EIRS- ASE-77-1, Mississippi State Univ.*, (1976).
- [22] Winslow A. M.: *J.Comp.Phys.*, 2 (1967), p. 149-172.
- [23] Costas D., Brian J.E, Kyung S.c., Beris A.N.: *J.of comp. Phys.*,144(1998), p. 517.